



Polyamidoamine dendrimers modified silica gel for uranium(VI) removal from aqueous solution using batch and fixed-bed column methods

A.F. Shaaban^{a,*}, A.A. Khalil^a, T.A. Lasheen^b, El Said A. Nouh^b, Huda Ammar^b

^aChemistry Department, Faculty of Science, Benha University, Benha, Egypt, Tel. +201091174238;

email: afshaaban@hotmail.com (A.F. Shaaban), Tel. +201063029888; email: aamkhalil55@yahoo.com (A.A. Khalil)

^bNuclear Materials Authority, El Maadi, Cairo, Egypt, Tel. +201224459718; email: TiTi_lasheen@yahoo.com (T.A. Lasheen),

Tel. +201221933719; email: saidnouh81@yahoo.com (E.S.A. Nouh), Tel. +201112156241; email: ammar.huda@yahoo.com (H. Ammar)

Received 17 June 2017; Accepted 12 December 2017

ABSTRACT

Different generations of modified silica gel with polyamidoamine (PAMAM) dendrimers were synthesized. The adsorbents were characterized using Fourier transform infrared, scanning electron microscopy with energy dispersive X-ray spectroscopy thermal gravimetric analysis and porous structure analysis. The uptake behavior of Si-6G PAMAM toward U(VI) at different experimental conditions of pH, time, temperature and concentration was studied using batch mode. The maximum adsorption capacity of Si-6G PAMAM was 303.03 mg g⁻¹ as described effectively by Langmuir isotherm model. Kinetics and thermodynamics studies of U(VI) adsorption onto Si-6G PAMAM showed an endothermic pseudo-second-order adsorption process. The experimental results in the column method were described by Thomas and Yoon–Nelson models under different operating conditions.

Keywords: Uranium; Adsorption; Silica gel; Polyamidoamine dendrimers; Fixed-bed column

1. Introduction

Uranium is a widely spread element in the environment. It is found in rocks, soil, black sand, rivers, oceans and microorganisms. Uranium is used in the civil sector as a fuel in commercial nuclear power plants. Also, it is used in various applications such as a nuclear weapon, electron microscope [1,2] and catalysis [3]. Large quantities of solid and liquid wastes are produced from these applications. Uranium wastes have a dangerous effect on human, animals and plants [4,5]. Many techniques such as solvent extraction [6], precipitation [7], electrochemical techniques [8], ion-exchange methods [9], flotation and coagulation have been used for removal of uranium from aqueous solution [4]. However, most of these methods suffer from their high cost, low efficiency and inapplicability for all pollutants [10].

Adsorption is one of the economic and the efficient separation method when it is combined with a suitable desorption step in order to solve the problem of sludge disposal [11–14]. Many sorbents have been used for removal of uranium from aqueous solutions; these sorbents include polymeric resins, functionalized chitosan, naphthalene activated carbon, silica gel, etc. [10,15–18]. Moreover, biosorption studies using living biomass as the alga *Chlorella vulgaris* was used for recovery and biosorption of U(VI) ions from aqueous solution [19].

Chemical modification of silica gel surface by organic groups eliminates many limitations such as low adsorption capacities, weak interactions with metals, adsorbents separation, and regeneration difficulties and increases the selectivity toward the metal ions more than that offered by the traditional ion-exchanger and other adsorbents [20,21]. Our previous studies described the preparation of different

* Corresponding author.

chelating resins bearing amidoxime, iminodiacetate and dithiocarbamate groups for removal of some metal ions from aqueous solution [22–24]. Dendrimers have many unique properties such as the empty spaces in its structure and a large number of the functional group. Different dendrimers were used in many important applications [10,25] as removal of uranium and other metal ions from aqueous solutions [26].

According to our knowledge, Si-6G PAMAM was not used before as adsorbent for removal of U(VI) from aqueous solution. Thereby in the present work, silica gel was easily synthesized from white sand then modified with polyamidoamine (PAMAM) dendrimers to finally form Si-6G PAMAM. The synthesized adsorbent (Si-6G PAMAM) showed unprecedented capacity toward U(VI) removal in both batch and column mode.

2. Materials and methods

2.1. Materials

3-Aminopropyltrimethoxysilane (APMS), methyl acrylate (MA), ethylenediamine (EDA) and Arsenazo III were obtained from Sigma-Aldrich, Germany. U(VI) stock solution (1,000 mg L⁻¹) was prepared by dissolving 2.11 g of UO₂(NO₃)₂·6H₂O (Sigma-Aldrich, Germany) in 1 L of 0.05 M HNO₃. Natural white sand was supplied from Abou Zniema, Sinai, Egypt. The white sand was purified by washing with hydrochloric acid (0.1 M), then washed with double distilled water and dried in air. The purity of the sand was found 99.5% as indicated in Table 1.

2.2. Synthesis of adsorbents

2.2.1. Preparation of silica gel

Sodium silicate was prepared by heating 10 g of white sands with 20 g of sodium carbonate at 800°C. The white powder material was dispersed in double distilled water to dissolve sodium silicate. The silica gel particles were obtained by dropwise addition of hydrochloric acid (2 M) to the diluted sodium silicate under continuous stirring until polymerization. The prepared silica gel was washed with double distilled water, dried at 100°C and stored in desiccators [27].

2.2.2. Preparation of silica gel modified with APMS (Si-AMPS)

Silica gel (50 g) was activated by reflux in 150 mL of hydrochloric acid (6 M) for 4 h then filtrated, repeatedly washed with double distilled water till be acid-free and finally dried in an oven at 160°C for 6 h. To a 500 mL flask containing

toluene, the activated silica gel (40 g) and APMS (45 mL) were added and refluxed for 8 h. The prepared Si-AMPS was filtered off, washed with ethanol and dried under vacuum at 70°C [5].

2.2.3. Preparation of Si-nG PAMAM

Si-nG PAMAM was prepared according to the modified method of Cao et al. [10]. To a 500 mL flask a mixture of Si-AMPS (40 g), MA (20 mL) and methanol (200 mL) was added and stirred at room temperature for 24 h under a nitrogen atmosphere to obtain half-generation modified silica gel (Si-0.5G PAMAM). After being filtered off, the half generation product was washed several times with ethanol and double distilled water followed by drying under vacuum at 50°C. Si-0.5G PAMAM was mixed with excess EDA (20 mL) and ethanol (200 mL), then the mixture was stirred at room temperature for 24 h to obtain the complete generation of modified silica gel (Si-1G PAMAM). Finally, the previous two steps were repeated to obtain different generations of modified silica gel (Si-nG PAMAM).

2.3. Characterization of silica gel and different generations of Si-nG PAMAM

The X-ray diffraction of the silica gel was obtained from Diano X-ray diffractometer using Cu K α radiation ($\lambda = 1.5418 \text{ \AA}$). Fourier transform infrared (FTIR) spectra of silica gel, Si-2G PAMAM, Si-4G PAMAM and Si-6G PAMAM before and after uranium adsorption were determined using Nexeus-Nicolite Model 640-MSA. Thermal gravimetric analysis (TGA) of silica gel, Si-4G PAMAM and Si-6G PAMAM were determined under N₂ atmosphere using temperature range from room temperature to 800°C and heating rate of 10°C min⁻¹ using SDT Q600 V20.5 Build 15. Surface morphology of Si-6G PAMAM before and after uranium adsorption was observed using SEM Model Quanta 250 FEG (Field Emission Gun) attached with EDX Unit. Porous structure parameters of white sand, silica gel, Si-3G PAMAM and Si-6G PAMAM were characterized by Brunauer–Emmett–Teller (BET) and Barrett–Joyner–Halenda (BJH) methods (Quantachrome Instruments v11.03) through N₂ adsorption–desorption methods using nitrogen gas as adsorbent at 77 K. Before analysis all adsorbents were pretreated in vacuum at 100°C for 2 h.

2.4. Uptake of U(VI) using batch method

The batch technique was carried out in a series of flasks. In each flask, 0.02–0.15 g of Si-6G PAMAM was added to 100 mL of uranium solution with initial concentration 70–800 mg g⁻¹. The flasks were shaken using a Vibromatic-384 shaker at 120 rpm for 1–60 min at 25°C, 35°C, and 40°C and pH range 2–9. The residual concentration of U(VI) at equilibration was analyzed spectrophotometrically using Arsenazo III [28] using a double-beam Jasco (UV-Visible) spectrophotometer (Japan). All experiments were carried out three times to check the reproducibility of each result.

The removal percentage (*R*) and the adsorption capacity (*Q_e*) for uranium were calculated according to Eqs. (1) and (2), respectively.

Table 1
Chemical analysis of white sand

Oxide	Concentration (%)
SiO ₂	99.50
Al ₂ O ₃	0.30
TiO ₂	0.03
Fe ₂ O ₃	0.16

$$R = \frac{C_0 - C_e}{C_0} \times 100\% \quad (1)$$

$$Q_e = \frac{(C_0 - C_e)V}{W} \quad (2)$$

where Q_e is the adsorption capacity (mg g^{-1}). C_0 and C_e are the initial and equilibrium uranium concentration (mg L^{-1}), respectively, V is the volume of uranium solution (L) and W is the weight of dry Si-6G PAMAM (g).

2.5. Uptake of U(VI) using column method

The synthesized Si-6G PAMAM was also examined in a fixed-bed column for the adsorption of U(VI). The experiments were accomplished in a glass column with an inner diameter of 1.0 cm and length of 10 cm packed with the prepared adsorbent at different bed heights (1 and 2 cm). U(VI) solution (pH 4.5, 100 mg L^{-1}) was pumped to the top of the column under the required flow rate (1, 3 and 5 mL min^{-1}). The outlets U(VI) concentration was collected at definite time intervals and analyzed. The column experiments were stopped when the outlet concentration of U(VI) equal the initial concentration.

The fixed-bed adsorption is conveniently described through the breakthrough curve C_{eff}/C_0 vs. volume (where C_{eff} and C_0 are the effluent and inlet metal ions concentration, respectively) for a given bed height. The value of total adsorbed U(VI) quantity of a given influent concentration and flow rate from the area under the breakthrough curve was determined by integrated the adsorbed U(VI) concentration vs. time as illustrated in the following equation [29]:

$$m_{\text{total}} = \frac{Q}{1,000} \int_0^{\text{tot}} C_{\text{ads}} dt = \frac{Q}{1,000} \int_0^{\text{tot}} (C_0 - C_{\text{eff}}) dt \quad (3)$$

where Q and C_{ads} are the volumetric flow rate (mL min^{-1}) and concentration of adsorbed metal ion (mg L^{-1}), respectively.

The equilibrium adsorption capacity q_e (mg g^{-1}) [29] is calculated from Eq. (4):

$$q_e = \frac{m_{\text{total}}}{W} \quad (4)$$

where W is the total dry weight of Si-6G PAMAM (g).

The total amount of uranium ion fed into the column (X , mg) is calculated from the following equation:

$$X = \frac{C_0 V_{\text{eff}}}{1,000} \quad (5)$$

where V_{eff} is the effluent volume of the uranium solution (mL).

The percentage removal of the U(VI) by the column, that is, the column performance by Si-6G PAMAM can be calculated from the following equation:

$$R(\%) = \frac{m_{\text{total}}}{M_{\text{total}}} \times 100 \quad (6)$$

Also, the mass transfer zone Δt is given by the following equation:

$$\Delta t = t_e - t_b \quad (7)$$

where t_b is the breakthrough time (which is the time needed for the increase of metal ion concentration in the effluent to an appreciable value in a sudden way) and t_e is the bed exhaustion time (which is the time needed for the increase of metal ion concentration in the effluent exceeding 99% of the influent concentration).

The length of mass transfer zone (Z_m , cm) is obtained from the breakthrough curve calculated from the following equation [30]:

$$Z_m = Z \left(1 - \frac{t_b}{t_e} \right) \quad (8)$$

where Z is the bed height in cm.

2.6. Elution experiment

Elution experiments were carried out by placing 0.25 g of Si-6G PAMAM in the column then loaded with U(VI) at the flow rate of 1 mL min^{-1} . The maximum uptake was obtained in the first run, thereafter the adsorbent was washed by flowing distilled water crossing the column. The synthesized adsorbent loaded by U(VI) was subjected to elution using 1 M HNO_3 , then washed carefully with a diluted aqueous solution of NaOH and finally with distilled water to become ready for using again.

3. Results and discussion

3.1. Synthesis and characterization of silica gel and different generations of Si-*n*G PAMAM

Modified silica gel Si-*n*G PAMAM was synthesized via different steps as described in Fig. 1.

The diffraction peaks of silica gel as shown in Fig. 2 about 24° , which was the amorphous diffraction peak of silica gel.

In the spectrum of silica gel (Fig. 3(a)), the broad band around $3,430 \text{ cm}^{-1}$ can be referred to the O–H stretching vibration of the free silanol group. The strong band of Si–O–Si stretching vibration appears at $1,100 \text{ cm}^{-1}$. In the spectrum of Si-*n*G PAMAM, the new bands appeared at $2,953$ and $2,852 \text{ cm}^{-1}$ corresponding to the asymmetric and symmetric CH_2 bands, indicating the presence of carbon chain on Si-*n*G PAMAM as illustrated in Fig. 3(b). The band at $1,735 \text{ cm}^{-1}$ suggested the presence of ester bonds ($-\text{CO}_2\text{CH}_3$) as shown in Fig. 3(c). With increasing the generation, the absorption at $1,735 \text{ cm}^{-1}$ disappeared, and two new infrared bands at $1,645$ and $1,566 \text{ cm}^{-1}$ have appeared. They were assigned to amide I and amide II groups (Fig. 3(d)).

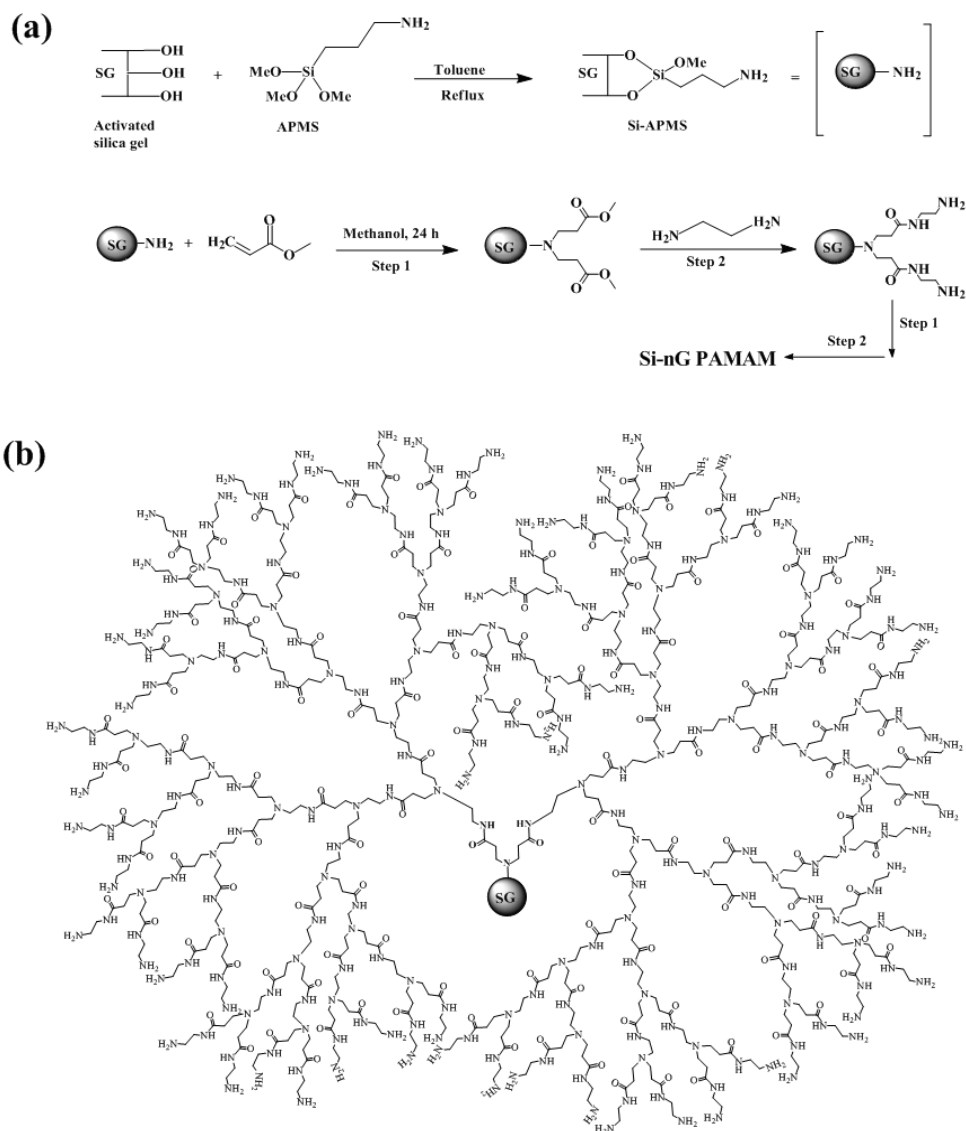


Fig. 1. The ideal synthetic routes of (a) Si-nG PAMAM and (b) the ideal product (Si-6G PAMAM).

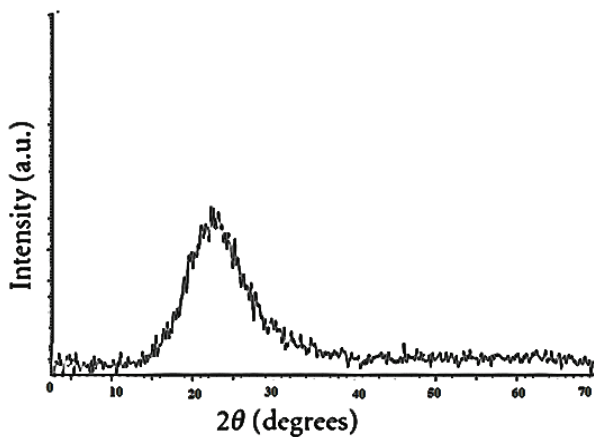


Fig. 2. X-ray powder diffraction patterns of silica gel.

By comparing the FTIR spectrum before and after U(VI) adsorption onto the Si-6G PAMAM, it is found that a new peak appearing at 924 cm⁻¹ (Fig. 3(e)) which belonged to the stretching vibrations of uranyl ions.

TGA was performed to give evidence about the thermal stability of prepared silica gel and its modified generations (Si-4G PAMAM and Si-6G PAMAM). As can be observed in Fig. 4, silica gel showed a first loss of 20.32% until 130°C due to physically adsorbed water and a second loss in the range of 130°C–800°C. On the other hand, the modified silica gel shows multistage thermogravimetric profiles. The release of adsorbed water at 130°C was 5.18% and 4.82% for Si-4G PAMAM and Si-6G PAMAM, respectively. The observed lower dehydration percentage in case of Si-4G PAMAM and Si-6G PAMAM than that of silica gel gave a confirmation about the lower affinity of modified silica gel toward water. The weight losses above 130°C are mainly attributed to the organic content of the samples.

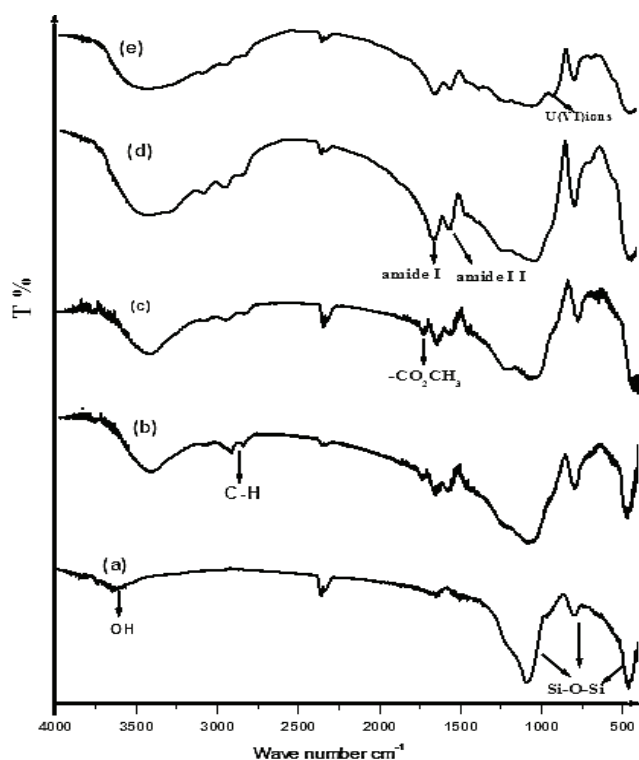


Fig. 3. FTIR spectra of (a) silica gel, (b) Si-2G PAMAM, (c) Si-4G PAMAM, (d) Si-6G PAMAM and (e) Si-6G PAMAM after U(VI) adsorption.

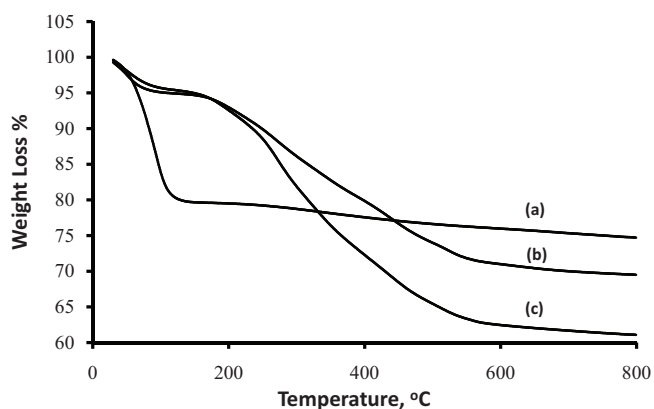


Fig. 4. TGA curves of (a) silica gel, (b) Si-4G PAMAM and (c) Si-6G PAMAM.

The BET surface area, BJH desorption cumulative volume of pores and BJH desorption average pore radius for white sand, silica gel, Si-3G PAMAM and Si-6G PAMAM were determined. The values of BET surface area, BJH desorption average pore radius and BJH desorption cumulative volume of pores for the products decreased by increasing the generations (Table 2). This may be attributed to the formation of PAMAM dendrimers in the pores of adsorbent, the volume of dendrimers was increased with the increasing of generation number, so the surface area and pore size of the prepared Si-6G PAMAM become smaller. This indicates that increasing the number of functional groups on Si-*n*G PAMAM surface might be more important than high surface area and high pore volume when the prepared adsorbent is used for adsorption [31].

The N₂ adsorption/desorption isotherms for white sand, silica gel, Si-3G PAMAM and Si-6G PAMAM are shown in Fig. 5. According to IUPAC classification [32], the adsorption/desorption isotherms of white sand, silica gel and Si-3G PAMAM were type IV with H2 hysteresis loops at P/P_0 range from 0.5 to 0.9 that is characteristic of mesoporous structures. But adsorption/desorption isotherm and hysteresis loops for Si-6G PAMAM was type V with H1 hysteresis loops at P/P_0 range from 0.5 to 0.9. This is indicating for mesoporous structure with uniform sphere. The volume of adsorbed nitrogen for all samples decreased with the proceeding of functionalization.

SEM images of Si-6G PAMAM before and after uranium adsorption are shown in Figs. 6(a) and (b) which demonstrates a change of the surface morphologies of the adsorbents. After adsorption of uranium, a lot of the crevices clearly are decreased and become separate which indicate that a certain amount of uranium ions has been adsorbed.

The EDX spectra (Figs. 6(c) and (d)) revealed the presence of the elements Si, O, C and N for Si-6G PAMAM before uranium adsorption (Fig. 6(c)). After adsorption process, we can see clearly the characteristic peaks of uranium (Fig. 6(d)).

3.2. Uptake of U(VI) by batch method

3.2.1. Effect of pH

The effect of pH on the uptake capacity of U(VI) for Si-6G PAMAM was investigated by shaking 0.1 g of the dry adsorbent with uranium solution (100 mL, 100 mg L⁻¹) for 1 h at 25°C at pH range 2–9. U(VI) is precipitated at high pH (pH values above 9) even from very low concentrations of uranyl nitrate [33]. As can be shown in Fig. 7, the adsorption capacity of Si-6G PAMAM increases with the increase of pH value until it reaches the maximum value at pH 4.5

Table 2

The parameters of porous structure of white sand, silica gel, Si-3G PAMAM and Si-6G PAMAM

Adsorbents	BET surface area (m ² g ⁻¹)	BJH desorption cumulative volume of pores (cm ³ g ⁻¹)	BJH desorption average pore radius (nm)
White sand	4,094.19	2.02	1.71
Silica gel	415.79	0.29	1.72
Si-3G PAMAM	130.25	0.42	3.92
Si-6G PAMAM	57.45	0.024	1.23

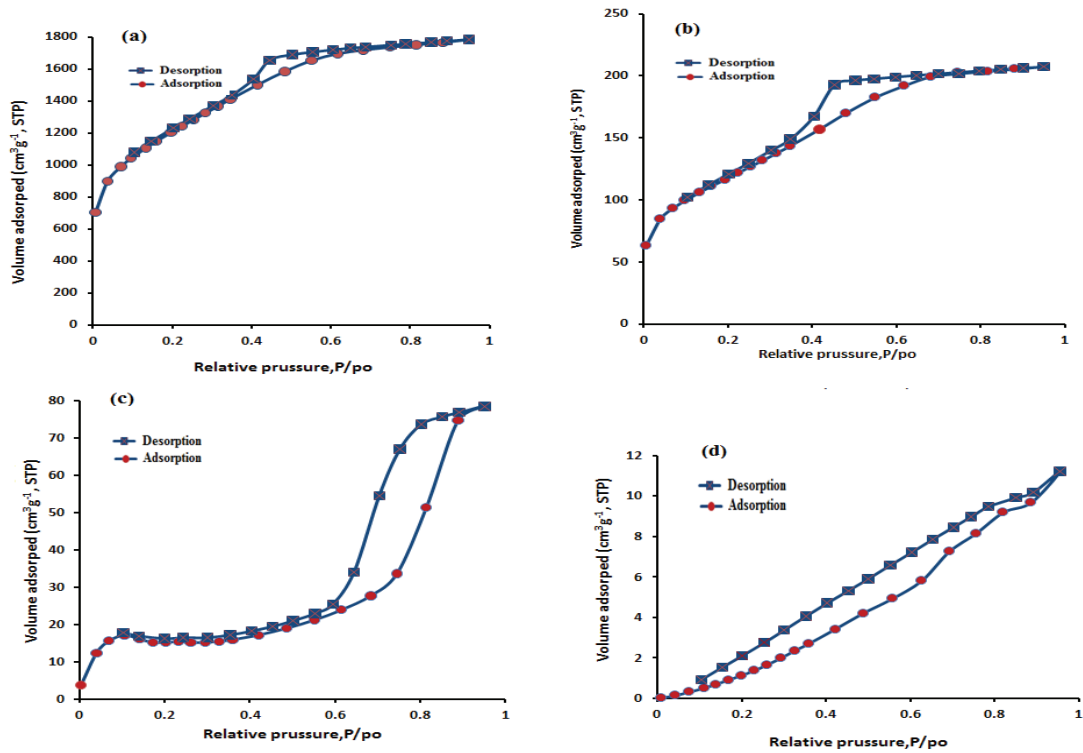


Fig. 5. Nitrogen adsorption–desorption isotherms of (a) white sand, (b) silica gel, (c) Si-3G PAMAM and (d) Si-6G PAMAM.

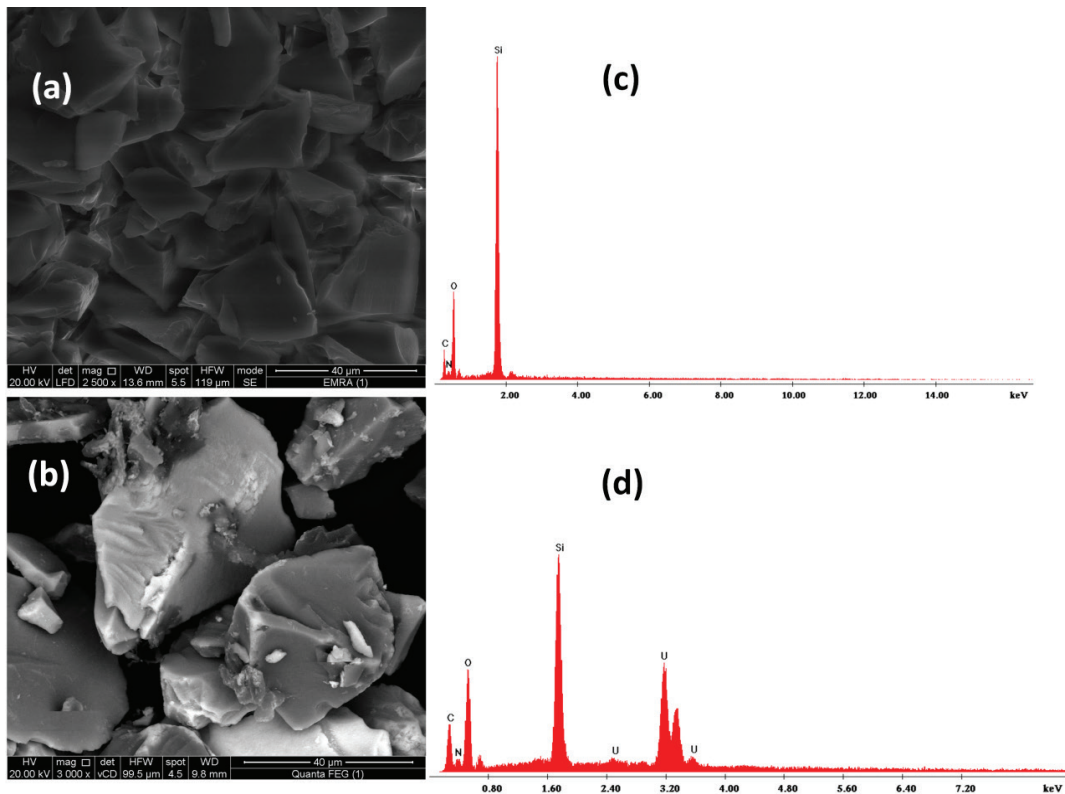


Fig. 6. SEM images of (a) and (b) Si-6G PAMAM before and after U(VI) adsorption, respectively, (c) and (d) the corresponding EDX for Si-6G PAMAM before and after U(VI) adsorption, respectively.

then decreases again. Actually, U(VI) presents in the solution in the form of UO_2^{2+} species. The modified silica gel has $-\text{NH}$ and $-\text{NH}_2$ groups which are responsible for a complex formation with uranium. The uranium adsorption at $\text{pH} \leq 4$ is observed to be less since primary and tertiary amino groups of Si-6G PAMAM are completely protonated and only amide functional groups are available for coordination with U(VI) ion. At lower pH, the predominant uranium species is UO_2^{2+} ion and its adsorption on the adsorbent is reduced due to the surface of Si-6G PAMAM exhibits increasing positive characteristics. At $\text{pH} \geq 4.8$ various oligomeric and monomeric hydrolyzed species of UO_2^{2+} are reported. These include $[\text{UO}_2\text{OH}]^+$, $[(\text{UO}_2)_3(\text{OH})_4]^{2+}$, $[(\text{UO}_2)_3(\text{OH})_5]^+$, $[(\text{UO}_2)_2(\text{OH})_2]^{2+}$, $[(\text{UO}_2)_2(\text{OH})_3]^+$, $[(\text{UO}_2)_3(\text{OH})_5]^{5+}$, $[(\text{UO}_2)_4(\text{OH})_7]^{7+}$, $[\text{UO}_2(\text{OH})_4]^{2-}$ and $[(\text{UO}_2)_3(\text{OH})_7]^-$ [32]. The uranium adsorption on Si-6G PAMAM was observed to be maximum at pH 4.5. In weakly acidic solution (pH 4–5.5), the hydrolysis products predominate in solution are $\text{UO}_2(\text{OH})^+$, $(\text{UO}_2)_2(\text{OH})_2^{2+}$ and $(\text{UO}_2)_3(\text{OH})_5^{5+}$ ions which are formed by the hydrolysis of UO_2^{2+} ions [34]. Deprotonation of amino groups and formation of various uranium hydrolysis products lead to increase in uranium adsorption at $\text{pH} > 4$. Also, negatively charged uranium species were found at higher pH values which cannot react with Si-6G PAMAM [20,28].

3.2.2. Effect of adsorbent amount

The experimental work was carried out over adsorbent amount in the range of 0.02–0.15 g and with the initial concentration of U(VI) (100 mg L^{-1} , 100 mL) at 25°C and pH 4.5. As can be illustrated in Fig. 8, the adsorption percentage of U(VI) increased with increasing Si-6G PAMAM dosage until 0.1 g which reached to 96%. After that, a tendency to show a plateau is observed.

3.2.3. Adsorption kinetics

The kinetics of adsorption have been studied to investigate the mechanism of adsorption, and to obtain the equilibrium time and the adsorption capacity. The kinetics experiments of U(VI) adsorption onto Si-6G PAMAM were performed at pH 4.5 using different temperature and different contact time with an initial concentration (100 mg L^{-1}). The equilibrium time was attended during 15 min as shown in Fig. 9. In order to discuss the kinetic mechanism which controls the adsorption process, two different kinetic models namely Lagergren's pseudo-first-order and pseudo-second-order kinetic models were used to fit the experimental data of U(VI) adsorption on Si-6G PAMAM. The mathematical expression of these models is illustrated in Eqs. (9) and (10) [35,36]:

$$\text{First-order model: } \ln(Q_e - Q_t) = \ln Q_e - \frac{K_1 t}{2.302} \quad (9)$$

$$\text{Second-order model: } \frac{t}{Q_t} = \frac{1}{K_2 Q_e^2} + \frac{t}{Q_e} \quad (10)$$

where K_1 (min^{-1}) and K_2 ($\text{g mg}^{-1} \text{ h}^{-1}$) are the adsorption rate constants for first-order and second-order equations,

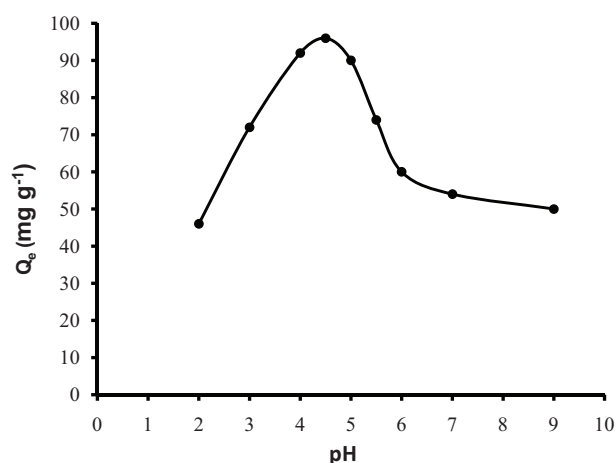


Fig. 7. Effect of pH on U(VI) uptake (U(VI): 100 mg L^{-1} , Si-6G PAMAM: 0.1 g, V: 100 mL and 25°C).

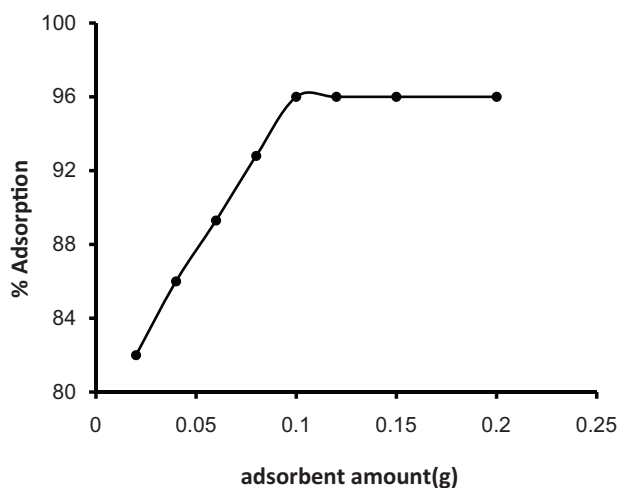


Fig. 8. Effect of Si-6G PAMAM amount on uptake of U(VI) (U(VI): 100 mg L^{-1} , pH: 4.5, V: 100 mL and 25°C).

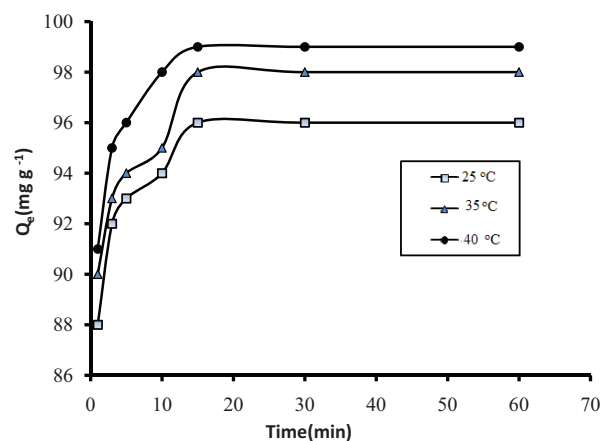


Fig. 9. Effect of contact time on the adsorption of U(VI) at different temperatures (U(VI): 100 mg L^{-1} , pH: 4.5, Si-6G PAMAM: 0.1 g, V: 100 mL).

respectively, t is the adsorption time (min); Q_e and Q_t are the adsorption capacity at equilibrium and at time t , respectively. The studied kinetic parameters of the pseudo-first-order and pseudo-second-order kinetic models are presented in Table 3. The obtained linear relationships in the case of the second-order kinetic model were extremely close to the experimental values ($R^2 = 1$) compared with those calculated by first-order kinetic model suggesting that the adsorption of U(VI) onto the Si-6G PAMAM obeys the second-order kinetic model.

3.2.4. Adsorption thermodynamic

Thermodynamic parameters of U(VI) adsorption process were estimated by performing the adsorption experiments at different temperatures (25°C, 35°C and 40°C). Uranium solution (100 mL, 100 mg L⁻¹) equilibrated with 0.1 g of Si-6G PAMAM at pH 4.5. Our results indicate that the adsorption of uranium onto Si-6G PAMAM increases by increasing the temperature. The thermodynamic parameters such as Gibbs energy (ΔG), enthalpy (ΔH) and entropy (ΔS) are calculated using the following equations [37,38]:

$$K_c = \frac{Q_e}{C_e} \quad (11)$$

$$\Delta G = \Delta H - T\Delta S \quad (12)$$

$$\ln K_c = \frac{\Delta S}{R} - \frac{\Delta H}{RT} \quad (13)$$

where K_c is the thermodynamic equilibrium constant, T is the temperature of solution (K) and R (8.314 J mol⁻¹ K⁻¹) is the universal gas constant. Enthalpy change (ΔH) and entropy (ΔS) were determined by plotting $\ln K_c$ vs. $1/T$ (Fig. 10) according to Van't Hoff Eq. (12). Free energy change (ΔG) is calculated using Eq. (11). As can be seen in Table 4, the positive value of ΔH means that the adsorption of uranium using Si-6G PAMAM is an endothermic process [39]. Also, ΔS gives the positive value which suggests an increase in randomness at the solid/liquid interface during the adsorption process. The negative value of free energy change (ΔG) proves the feasibility and the spontaneous nature of uranium adsorption into Si-6G PAMAM. The negative values of ΔG are increased by increasing the temperature which indicate the formation of more stable bonding between U(VI) and amino groups of Si-6G PAMAM at the higher temperature, consequently more adsorption capacity.

Table 3
Kinetic parameter for U(VI) adsorption onto Si-6G PAMAM

Equations	Parameters	Temperature		
		25°C	35°C	40°C
Pseudo-first-order kinetic	Q_e (mg g ⁻¹)	7.27	6.23	8.78
	K_1 (min ⁻¹)	0.32	0.21	0.51
	R^2	0.87	0.53	0.98
Pseudo-second-order kinetic	Q_e (mg g ⁻¹)	96.15	98.04	99.01
	K_2 (g mg ⁻¹ h ⁻¹)	0.08	0.06	0.09
	R^2	1	1	1

3.2.5. Effect of initial concentration and equilibrium isotherm models

The effect of initial U(VI) concentration on the adsorption capacity of Si-6G PAMAM was studied in the concentration range (70–800 mg L⁻¹) at pH 4.5 at 25°C. As shown in Fig. 11, the adsorption capacity of Si-6G PAMAM increases by increasing U(VI) initial concentration until reaching the plateau.

The adsorption isotherm of Si-6G PAMAM for U(VI) was discussed by Langmuir, Freundlich and Temkin models. The linear form of Langmuir adsorption model can be represented as described in Eq. (14) [40]:

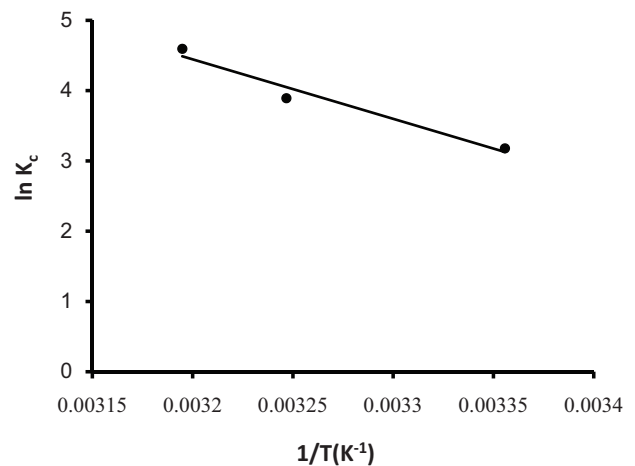


Fig. 10. Plot of $\ln K_c$ vs. $1/T$ for uranium adsorption into Si-6G PAMAM.

Table 4
Thermodynamic parameter for uranium adsorption onto Si-6G PAMAM

$-\Delta G$ (kJ mol ⁻¹)			ΔH (kJ mol ⁻¹)	ΔS (J(mol K) ⁻¹)
25°C	35°C	40°C		
7.76	10.38	11.69	70.36	262.14

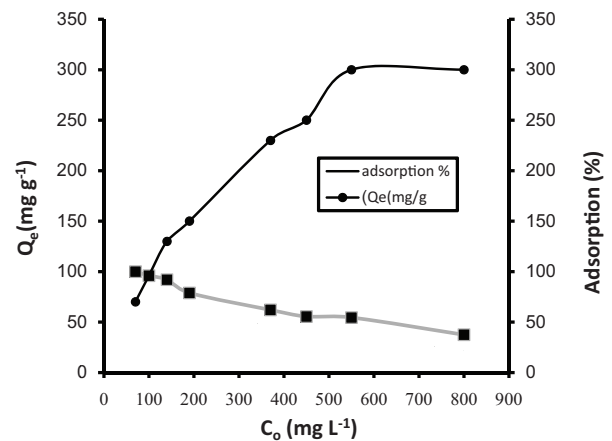


Fig. 11. Effect of initial concentration on uptake of U(VI) (pH: 4.5, Si-6G PAMAM: 0.1 g, V: 100 mL and 25°C).

$$\frac{C_e}{Q_e} = \frac{1}{bQ_{\max}} + \frac{C_e}{Q_{\max}} \quad (14)$$

where C_e is the equilibrium concentration of U(VI) in the solution (mg L^{-1}), Q_e is the adsorption capacity (mg g^{-1}) at equilibrium, Q_{\max} is the maximum adsorption capacity (mg g^{-1}) and b (L mg^{-1}) is the binding constant. According to Langmuir isotherm model (Fig. 12), the adsorption process is homogeneous, where adsorption activation energy on the surface of Si-6G PAMAM is uniform. Comparing with the results reported by different investigators, in our work the uptake capacity is considered as a good achievement (Table 5). Langmuir adsorption isotherm can be expressed in terms of a dimensionless constant called equilibrium parameter R_L which is defined as the following equation:

$$R_L = \frac{1}{1 + bC_0} \quad (15)$$

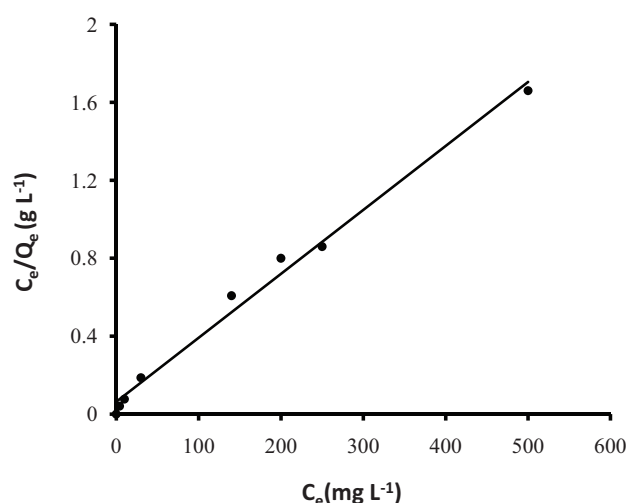


Fig. 12. Langmuir isotherm for the adsorption of U(VI) onto Si-6G PAMAM at 25°C.

Table 5

Comparison of maximum adsorption capacity of Si-6G PAMAM among other adsorbents reported in literature for the adsorption of U(VI)

Adsorbents	Adsorption capacity (mg g^{-1})	Conditions	Reference
Free silica gel	21.40	pH = 6.67, 25°C	[41]
Amberlite XAD-4-OVSC	2.38	pH = 6–8, 25°C	[42]
XAD-4-bicine resin	90.44	pH = 7.67, 25°C	[43]
Nanoporous silica	29.40	pH = 4, 22°C	[44]
PNIPAAm/CS semi-IPN hydrogels	2.86	pH = 5, 20°C	[45]
Triamine modified silica (TAMS)	90.30	pH = 4.5, 25°C	[46]
Pentamine modified silica (PAMS)	112.00	pH = 4.5, 25°C	[46]
Wheat straw	19.23	pH = 3, 30°C	[47]
4-Vinylpyridine-grafted-vinyltriethoxysilane-cellulose	134.00	pH = 7, 30°C	[48]
Si-6G PAMAM	303.03	pH = 4.5, 25°C	This work

The value of R_L indicates the nature of the isotherm to be unfavorable ($R_L > 1$), linear ($R_L = 1$), favorable ($0 < R_L < 1$) or irreversible ($R_L = 0$) [1,20]. Plotting R_L vs. C_0 is shown in Fig. 13, the calculated R_L values were found between 0 and 1. This indicates that the adsorption of U(VI) onto Si-6G PAMAM is favorable under the used conditions in this study. The R_L values decreased as the C_0 of uranium ion increased which showed that the adsorption of metal ions is more effective at higher initial concentration.

The Freundlich isotherm model (as shown in Fig. 14) is an empirical relation between the concentration of U(VI) on the surface of Si-6G PAMAM to the concentration of the U(VI) in the solution which is used to characterize heterogeneous adsorption system. The linear form of Freundlich adsorption model can be written as illustrated in the following equation [49]:

$$\ln Q_e = \ln K_f + \frac{\ln C_e}{n} \quad (16)$$

where K_f and n are constants for Freundlich adsorption model. Like R_L values of Langmuir isotherm model the values $1/n$ in Freundlich isotherm model indicates that the nature of isotherm to be unfavorable ($1/n > 1$), favorable ($0 < 1/n < 1$) or irreversible ($1/n = 0$), where $1/n$ values were found between 0 and 1, this means that the adsorption of U(VI) onto Si-6G PAMAM is favorable.

The Temkin isotherm model (Fig. 15) is represented by the following equation [50]:

$$Q_e = B_T \ln A_T + B_T \ln C_e \quad (17)$$

where $B_T = R_T/b_T$, T is the absolute temperature, R is universal gas constant, b_T is concerning to the heat of adsorption and A_T is the equilibrium binding constant. The values of Langmuir, Freundlich and Temkin equation parameters are tabulated in Table 6. Langmuir model shows better results than Freundlich and Temkin models because of the higher correlation coefficient for uranium ions.

3.2.6. Effect of dendron generation

Niu et al. [51] and Song et al. [52] confirmed that the increasing of generation number of PAMAM dendrimers results to the increasing number of functional groups, promoting the higher adsorption capacity when generation number was not more than 2. The high cross-linking structure and steric hindrance make it is difficult for metal ions to diffuse into the interior structure of PAMAM dendrimer, which contribute to the decrease of adsorption capacity. In contrary of that Laiyaraja et al. [20] confirmed that the adsorption capacity increased with the increasing generation

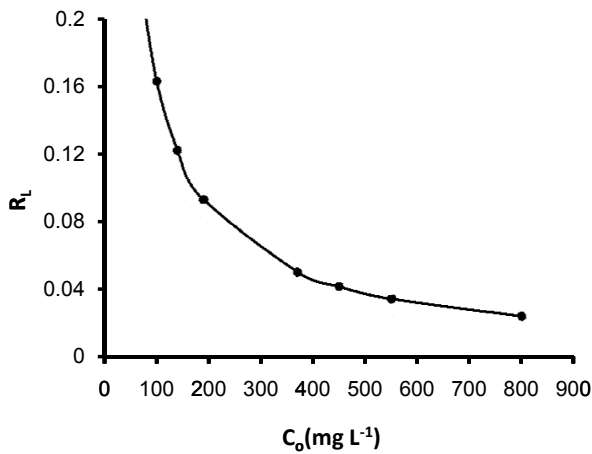


Fig. 13. Variation of adsorption intensity (R_L) with initial concentration (C_0) of U(VI).

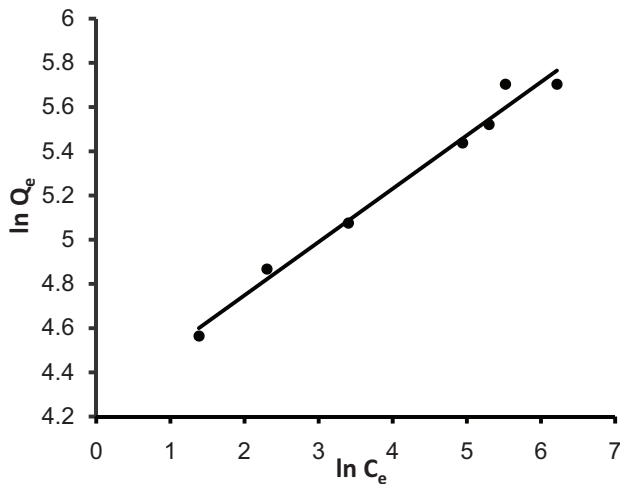


Fig. 14. Freundlich isotherm for the adsorption of U(VI) onto Si-6G PAMAM at 25°C.

Table 6 Adsorption isotherm parameters for U(VI) adsorption onto Si-6G PAMAM

Langmuir isotherm			Freundlich isotherm			Temkin isotherm			
Q_{max} (mg g ⁻¹)	B (L mg ⁻¹)	R^2	K_f	$1/n$	R^2	b_T	B_T (J mol ⁻¹)	A_T (L min ⁻¹)	R^2
303.03	0.051	0.99	71.25	0.24	0.98	0.19	44.23	1.79	0.96

number of PAMAM dendrimers. The reason for this was that the number of functional groups and binding sites increase with the increasing of generation number and thus the adsorption capacity was increased. As shown in Fig. 16, the maximum adsorption capacities of Si-1G PAMAM, Si-3G PAMAM, Si-5G PAMAM and Si-6G PAMAM at pH 4.5 were determined to be 129.77, 149.89, 238.34 and 300 mg g⁻¹, respectively, indicating the linear increase in adsorption with the increase in PAMAM dendron generation.

3.3. Uptake of U(VI) using fixed-bed column technique

The breakthrough curves (C_{eff}/C_0 vs. volume) of U(VI) adsorption onto Si-6G PAMAM are shown in Figs. 17(a)–(c) at bed height (1 and 2 cm) and flow rate (1, 3 and 5 mL min⁻¹) using initial U(VI) concentration of 100 mg L⁻¹ at pH 4.5.

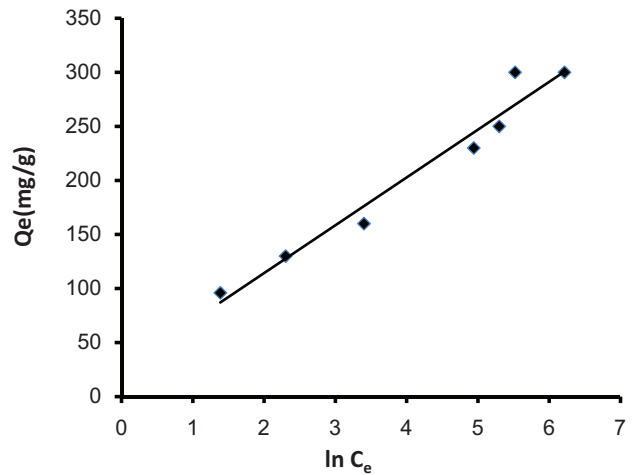


Fig. 15. Temkin isotherm for the adsorption of U(VI) onto Si-6G PAMAM at 25°C.

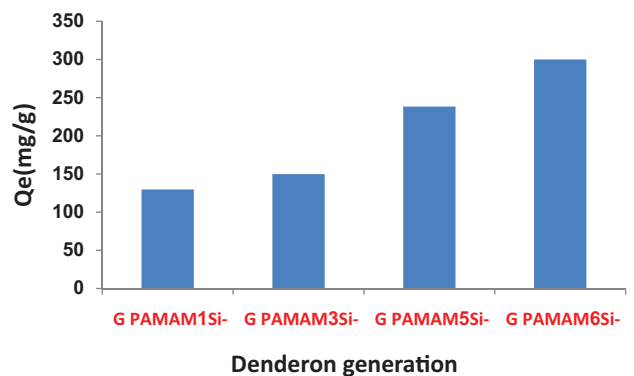


Fig. 16. Effect of PAMAM dendron generation on uranium adsorption capacity.

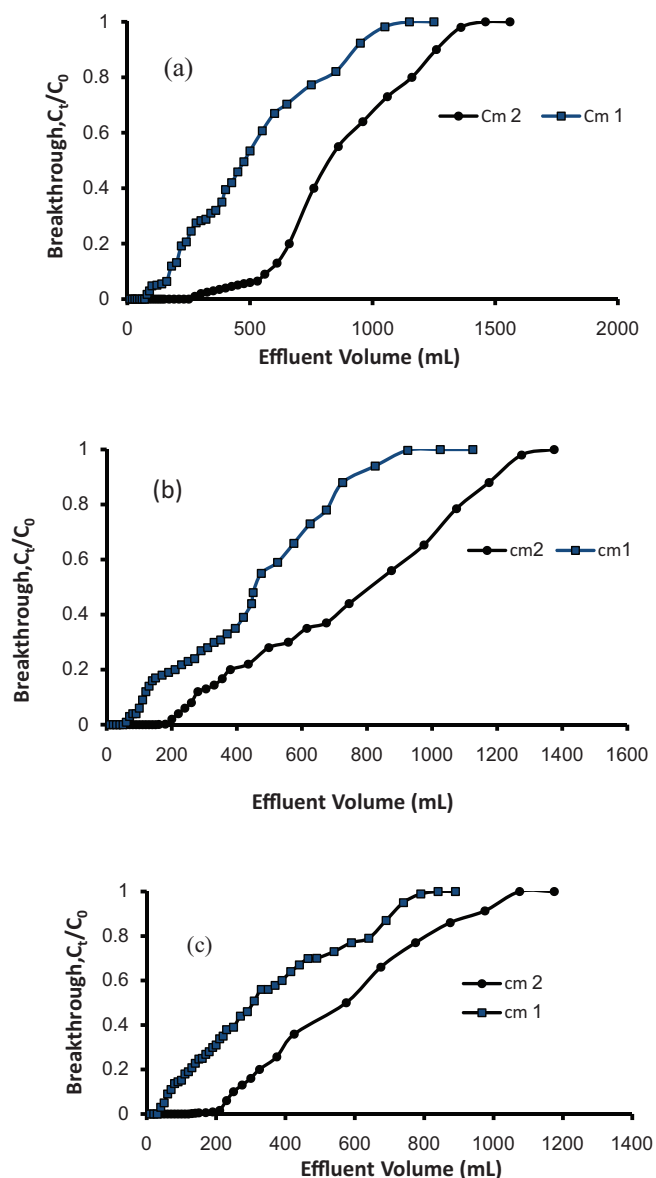


Fig. 17. The breakthrough curves of U(VI) adsorption at column bed height 1 and 2 cm. (a) 1 mL min⁻¹, (b) 3 mL min⁻¹ and (c) 5 mL min⁻¹ (U(VI): 100 mg L⁻¹, pH: 4.5 and 25°C).

The adsorption capacity of Si-6G PAMAM (q_e), removal percentage ($R\%$), the breakthrough time (t_b), exhaustion time (t_e), mass transfer zone Δt and the length of mass transfer zone (Z_m) were calculated from the breakthrough curves using Eqs. (3)–(8) and presented in Table 7. From this results, Si-6G PAMAM showed a higher adsorption capacity for U(VI). The maximum sorption capacity was 200.57 mg g⁻¹ at bed height 1 cm and flow rate 1 mL min⁻¹.

3.3.1. Effect of bed height

The shape of breakthrough curves of sorption of U(VI) (Figs. 17(a)–(c)) at flow rates (1, 3 and 5 mL min⁻¹) is significantly different at bed height (1 and 2 cm). In different curves, the adsorption of U(VI) continued after the breakthrough point and the C_{eff}/C_0 would increase rapidly then steadily moves forming the S-shaped curve. As shown in Table 7, the breakthrough time (t_b), exhaustion time (t_e) and mass transfer zone (Δt) were increased with increased in bed heights. This may be due to the amount of Si-6G PAMAM was more to contact U(VI). Also, the removal percentage of uranium ($R\%$) and the height of mass transfer zone (Z_m) were increased with increase in bed heights. In addition, a larger volume of metal uranium solution could be treated, as there was increased in the ratio of the adsorbent, whereas extra binding sites are ready for adsorption. The increase in percentage removal must be related to the maximum saturation of all active sites in the adsorbent dosage by metal ions and broad ended mass transfer zone. From the calculated results, it is clearly appeared that there are decreasing in uptake capacities (q_e , mg g⁻¹) by increasing the bed height is owing to the change in volume to mass ratio of ion exchange [53]. The sorption capacity of Si-6G PAMAM for U(VI) was calculated as about (200.57 mg g⁻¹) at bed height 1 cm and flow rate 1 mL min⁻¹ in fixed-bed column test and its value was lower than that of the batch test (303.03 mg g⁻¹). The difference can be explained as the insufficient contact time given for the sorption between uranium and Si-6G PAMAM under the fixed-bed column technique, as compared with batch technique [53].

3.3.2. Effect of flow rate

The flow rate also affected the shape of the breakthrough curve. As can be seen in Figs. 14(a)–(c) at the higher flow rate, the breakthrough time (t_b) and exhaustion time (t_e) reached

Table 7
Column data parameters, Thomas, Yoon–Nelson models constants for uranium adsorption at different conditions

Variables		Calculated parameter								Thomas model		Yoon–Nelson model			
Q (mL min ⁻¹)	Z (cm)	m_{total} (mg)	q_e (mg g ⁻¹)	R%	t_b (min)	t_e (min)	Δt (min)	Z_m (cm)	τ_{exp} (min)	q_0 (mg g ⁻¹)	K_{th} (mL mg ⁻¹ min ⁻¹)	R^2	K_{YN} (min ⁻¹)	τ (min)	R^2
1	1	50.14	200.57	40.11	70	1,150	1,080	0.873	478.21	201.77	0.067	0.94	0.0067	504.44	0.94
1	2	86.34	172.60	55.35	250	1,460	1,210	1.66	826.67	177.11	0.068	0.99	0.0068	885.5	0.99
3	1	44.92	179.68	39.92	16.66	341.66	325	0.95	152.38	174.50	0.24	0.91	0.024	145.68	0.91
3	2	75.78	151.56	51.37	50	458.33	408.33	1.76	269.98	154.80	0.14	0.93	0.014	260	0.93
5	1	34.61	138.44	38.88	6	168	162	0.95	61.33	129.71	0.35	0.95	0.035	64.88	0.95
5	2	56.45	112.90	48.04	24	215	191	1.78	115	122.50	0.46	0.85	0.046	122.50	0.85

more rapid (Table 7) and this may be due to the inadequate residence time of the U(VI) with Si-6G PAMAM and the reduced contact time causing a little distribution of the liquid inside the column [54]. The steeper breakthrough curve is observed at a higher flow rate, donating a more prominent effect of intraparticle diffusion and shorter service time of fixed-bed column. On the other hand, increasing flow rate from 1 to 5 mL min⁻¹ leads to decreasing the percentage of U(VI) removal (Table 7) for the reason that U(VI) left the column before reaching equilibrium. Also, the uranium sorption capacity (q_e , mg g⁻¹) decreases with increase in flow rate. Due to a longer time is needed between the solute and that of the solid phase to reach equilibrium state. Therefore, this increase in flow rate causes a presence of shorter time of the solute in the column and so, not all the metal ions will have enough time to penetrate from the solution to the modified silica and bind with dendrimer-amines functional groups [55]. The metal ion leaves the column rapidly before equilibrium occurs [56]. In general, the adsorption of U(VI) increased as the contact time increased provided at the lower flow rate.

3.3.3. Fixed-bed column models

Thomas and Yoon–Nelson models are theoretical models which used to test the experimental data related to the solute interaction behavior and to estimate the breakthrough curves.

3.3.3.1. Thomas model This model is a general model and widely used to describe column performance. The Thomas model is based on the assumption that the adsorption behavior follows Langmuir kinetics and assumes that the rate driving forces conforms to the second-order reversible reaction kinetics. This model can be represented by Eq. (18) [57]:

$$\frac{C_{\text{eff}}}{C_0} = 1 / 1 + \exp\left(\frac{K_{\text{th}}}{Q}(q_0 M - C_0 V_{\text{eff}})\right) \quad (18)$$

where C_{eff} is the effluent metal ion concentration (mg L⁻¹), K_{th} is Thomas rate constant (mL mg⁻¹ min⁻¹), q_0 is the equilibrium adsorbate uptake (mg g⁻¹), M is the adsorbent amount in the column (g), V_{eff} is the effluent volume of the solution (mL) and Q is volumetric flow rate (mL min⁻¹).

The linear form of this model is represented as:

$$\ln(C_{\text{eff}} / C_0 - 1) = \left[\frac{K_{\text{th}} q_0 M}{Q} - \frac{K_{\text{th}} C_0 V_{\text{eff}}}{Q} \right] \quad (19)$$

The values of K_{th} and q_0 can be determined from the slope and intercept of the linear graph between $\ln C_{\text{eff}}/C_0$ vs. V_{eff} at different flow rates and bed heights (Table 7). As can be observed, the calculated adsorption capacity of Si-6G PAMAM (q_0) from Thomas model is similar to the experimental adsorption capacity (q_e), our results are in good agreement with theoretical results. Also, the value of q_0 decreased with increasing flow rate and bed height.

3.3.3.2. Yoon–Nelson model This model used to describe the adsorption and breakthrough curves for adsorption of uranium ions onto Si-6G PAMAM in fixed-bed column and based on the concept of the decrease in the adsorption for each adsorbate molecule is directly proportional to the probability of adsorbate breakthrough on the adsorbent. This model can be represented as:

$$\frac{C_{\text{eff}}}{C_0 - C_{\text{eff}}} = \exp(K_{\text{YN}} t - \tau K_{\text{YN}}) \quad (20)$$

where K_{YN} is the kinetic adsorption rate constant (min⁻¹); t is the breakthrough time (min) and τ is the time required for 50% adsorbate breakthrough (min).

The linear form of this model is represented as:

$$\ln \frac{C_{\text{eff}}}{C_0 - C_{\text{eff}}} = K_{\text{YN}} t - \tau K_{\text{YN}} \quad (21)$$

The values of K_{YN} and τ can be calculated from a plot of $(\ln C_{\text{eff}}/C_0 - C_{\text{eff}} \text{ vs. } t)$ at different flow rates, and bed heights [58]. The values of K_{YN} , τ were tabulated in Table 7. The results show that K_{YN} increased with increasing flow rate and bed height. The data also indicate that the values of τ and τ_{exp} are close to each other. The observed increase in the value of the time required for 50% adsorbate breakthrough (τ) for U(VI) with increasing the bed height but the value of (τ) decreases with increasing the flow rate, due to less residence time of uranium ions in adsorbent bed [59]. It was observed that Thomas and Yoon–Nelson models were appropriate for describing all or a specific part of the dynamic behavior of continuous operation. The linearized equations of Thomas and Yoon–Nelson models can be written as shown in Eqs. (20) and (21). The equations indicate that both models have the same R^2 values and predicted breakthrough curve. Thomas model, analyzes the effect of adsorption capacity, on the other hand, the Yoon–Nelson model predicts the time required for 50% breakthrough. These data help to illustrate the efficiency of each individual model.

3.4. Desorption

The regeneration of the loaded Si-6G PAMAM by U(VI) was achieved using 1 M HNO₃ at 25°C. To check the reusability of Si-6G PAMAM, five successive adsorption–desorption cycles were performed according to the following equation [46]:

$$\text{Regeneration efficiency \%} = \frac{\text{Uptake of metal ion in the second cycle}}{\text{Uptake of metal ion in the first cycle}} \times 100 \quad (22)$$

From the uptake–elution process, it is clear that the adsorption capacity of newly prepared Si-6G PAMAM was hardly affected even after repeated five regeneration cycles. The adsorption capacity decreased from 100% to 99%, 98%, 97%, 95% and 93%, respectively, over five cycles.

4. Conclusion

Si-6G PAMAM was used for adsorption of U(VI) from aqueous solution. The Langmuir isotherm predicted the maximum adsorption capacity of Si-6G PAMAM to be 303.03 mg g⁻¹ at 25°C. The adsorption kinetics of Si-6G PAMAM followed the pseudo-second-order process. The calculated thermodynamic parameters (ΔG , ΔH and ΔS) indicate that the adsorption of U(VI) onto Si-6G PAMAM was spontaneous, endothermic and favorable. The breakthrough curves were obtained for U(VI) adsorption onto Si-6G PAMAM at different bed depth and influent flow rates. Thomas and Yoon–Nelson models were applied to experimental data and to determine the column kinetic parameters. The maximum adsorption capacity of Si-6G PAM in column studies was 201.77 at bed height 1 cm and flow rate 1 mL min⁻¹. The time required for 50% adsorbate breakthrough (τ) for U(VI) decreased with increasing flow rate but increased with increasing bed height of Si-6G PAMAM. Finally, it can be concluded that Si-6G PAMAM is a good adsorbent for adsorption of U(VI) ions from aqueous due to its efficiency and durability.

References

- [1] A.M. Donia, A.A. Atia, E.M.M. Moussa, A.M. El-Sherif, M.O. Abd El-Magied, Removal of uranium(VI) from aqueous solutions using glycidyl methacrylate chelating resins, *Hydrometallurgy*, 95 (2009) 183–189.
- [2] M. Eisenbud, T. Gesell, *Environmental Radioactivity from Natural, Industrial, and Military Sources*, Academic Press, Elsevier Science Publishing Co Inc, 1997.
- [3] S.H. Taylor, C.S. Heneghan, G.J. Hutchings, I.D. Hudson, The activity and mechanism of uranium oxide catalysts for the oxidative destruction of volatile organic compounds, *Catal. Today*, 59 (2000) 249–259.
- [4] T.P. Rao, P. Metilda, J.M. Gladis, Preconcentration techniques for uranium(VI) and thorium(IV) prior to analytical determination, *Talanta*, 68 (2006) 1047–1064.
- [5] S. Sadeghi, E. Sheikhzadeh, Solid phase extraction using silica gel modified with murexide for preconcentration of uranium(VI) ions from water samples, *J. Hazard. Mater.*, 163 (2009) 861–868.
- [6] Y.K. Agrawal, P. Shrivatav, S.K. Mnem, Solvent extraction separation of uranium(VI) with crown ether, *Sep. Purif. Technol.*, 20 (2000) 177–183.
- [7] A. Mellah, S. Chegrouche, M. Barkat, The precipitation of ammonium uranyl carbonate (AUC): thermodynamic and kinetic investigations, *Hydrometallurgy*, 85 (2007) 163–171.
- [8] C.S. Wang, Y. Liu, H. He, F.X. Gao, L.S. Liu, S.W. Chang, J.H. Guo, L. Chang, R.X. Li, Y.G. Ouyang, Electrochemical separation of uranium and cerium in molten LiCl–KCl, *J. Radioanal. Nucl. Chem.*, 298 (2013) 581–586.
- [9] A.C. Ladeira, C.A. Morais, Uranium recovery from industrial effluent by ion exchange – column experiments, *Miner. Eng.*, 18 (2005) 1337–1340.
- [10] Q. Cao, Y. Liu, C. Wang, J. Cheng, Phosphorous-modified poly(styrene-co-divinyl benzene)-PAMAM chelating resin for the adsorption of uranium(VI) in aqueous, *J. Hazard. Mater.*, 263 (2013) 311–321.
- [11] B. Samiey, C. Cheng, J. Wu, Organic-inorganic hybrid polymers as adsorbents for removal of heavy metal ions from solutions: a review, *Materials*, 7 (2014) 673–726.
- [12] B.J. Pan, B.C. Pan, M.W. Zhang, L. Lv, Q.X. Zhang, S.R. Zheng, Development of polymeric and polymer-based hybrid adsorbents for pollutants removal from waters, *Chem. Eng. J.*, 151 (2009) 19–29.
- [13] F. Ke, L.G. Qiu, Y.P. Yuana, F.M. Penga, X. Jianga, A.J. Xiea, Y.H. Shena, J.F. Zhuh, Thiol-functionalization of metal-organic framework by a facile coordination-based postsynthetic strategy and enhanced removal of Hg²⁺ from water, *J. Hazard. Mater.*, 196 (2011) 36–43.
- [14] Y. Niu, R. Qu, H. Chen, L. Mu, X. Liu, T. Wang, Y. Zhang, C. Sun, Synthesis of silica gel supported salicylaldehyde modified PAMAM dendrimers for the effective removal of Hg(II) from aqueous solution, *J. Hazard. Mater.*, 278 (2014) 267–278.
- [15] M. Jansson-Charrier, E. Guibel, J. Roussy, R. Surgons, P. Le Cloirec, Dynamic removal of uranium by chitosan: influence of operating parameters, *Water Sci. Technol.*, 34 (1996) 169–177.
- [16] A.A. Atea, Studies on interaction of mercury(II) and uranyl(II) with modified chitosan resins, *Hydrometallurgy*, 80 (2005) 13–22.
- [17] B.L. Rivas, H.A. Maturama, X. Ocampo, I.M. Peric, Adsorption behavior of Cu²⁺ and UO₂²⁺ ions on crosslinked poly[2,2-bis(acrylamido)acetic acid], *J. Appl. Polym. Sci.*, 58 (1995) 2201–2205.
- [18] U. Ulusoy, S. Simsek, O. Ceyhan, Investigations for modifications of poly acrylamide-bentonite by phytic acid and its usability in Fe³⁺, Zn²⁺ and UO₂²⁺ adsorption, *Adsorption*, 9 (2003) 165–175.
- [19] M. Amiri, H. Younesi, N. Bahramifar, Biosorption of U(VI) from aqueous solution by *Chlorella vulgaris*: equilibrium, kinetic and thermodynamic studies, *J. Environ. Eng.*, 139 (2013) 410–421.
- [20] P. Laiyara, A.K. Deb, K. Sivasubramanian, D. Ponraju, B. Venkatraman, Adsorption of uranium from aqueous solution by PAMAM dendron functionalized styrene divinylbenzene, *J. Hazard. Mater.*, 250–251 (2013) 155–166.
- [21] M. Zougagh, J.M. Cano Pavo, A. Garcia de Torres, Chelating sorbents based on silica gel and their application in atomic spectrometry, *Anal. Bioanal. Chem.*, 381 (2005) 1103–1113.
- [22] A.F. Shaaban, D.A. Fadel, A.A. Mahmoud, M.A. Elkomy, S.M. Elbahi, Synthesis of a new chelating resin bearing amidoxime group for adsorption of Cu(II), Ni(II) and Pb(II) by batch and fixed-bed column methods, *J. Environ. Chem. Eng.*, 2 (2014) 632–641.
- [23] A.F. Shaaban, D.A. Fadel, A.A. Mahmoud, M.A. Elkomy, S.M. Elbahi, Removal of Pb(II), Cd(II), Mn(II) and Zn(II) using iminodiacetate chelating resin by batch and fixed bed column methods, *Desal. Wat. Treat.*, 51 (2013) 5526–5536.
- [24] A.F. Shaaban, D.A. Fadel, A.A. Mahmoud, M.A. Elkomy, S.M. Elbahi, Synthesis and characterization of dithiocarbamate chelating resin and its adsorption performance towards Hg(II), Cd(II) and Pb(II) by batch and fixed-bed column methods, *J. Environ. Chem. Eng.*, 1 (2013) 208–217.
- [25] H.N. Patel, P.M. Patel, Dendrimer application a review, *Int. J. Pharm. Biol. Sci.*, 4 (2013) 454–463.
- [26] B. Klajnert, M. Bryszewska, Dendrimers: properties and applications, *Acta Biochim. Pol.*, 48 (2001) 199–208.
- [27] A. Sdiri, T. Higashi, S. Bouaziz, M. Benzina, Synthesis and characterization of silica gel from siliceous sands of southern Tunisia, *Arabian J. Chem.*, 7 (2014) 486–493.
- [28] Z. Marzenko, *Separation and Spectrophotometric Determination of Elements*, Ellis Harwood, Chichester, 1986.
- [29] A.M. El-Kamash, Evaluation of zeolite A for the sorptive removal of Cs⁺ and Sr⁺ ions from aqueous solutions using batch and fixed bed column operations, *J. Hazard. Mater.*, 151 (2008) 432–445.
- [30] C.M. Futralan, C.C. Kan, M.L. Dalida, C. Pascua, M.W. Wan, Fixed-bed column studies on the removal of copper using chitosan immobilized on bentonite, *Carbohydr. Polym.*, 83 (2011) 697–704.
- [31] Q. Qu, Q. Gu, Z. Gu, Y. Shen, C. Wang, X. Hu, Efficient removal of heavy metal from aqueous solution by sulfonic acid functionalized nonporous silica microspheres, *Colloids Surf., A*, 415 (2012) 41–46.
- [32] G. Meinrath, Aquatic chemistry of uranium, *Geoscience*, 1 (1998) 1–101.
- [33] B. Tomažič, M. Braniča, B. Težak, Precipitation and Hydrolysis of Uranium(VI) in aqueous solutions: uranyl nitrate-potassium hydroxide-neutral electrolyte, *Croat. Chem. Acta*, 34 (1962) (41–50).
- [34] T.S. Anirudhan, S.S. Sreekmari, Synthesis and characterization of a functionalized graft copolymer of densified cellulose for

- the extraction of uranium(VI) from aqueous solutions, *Colloids Surf., A*, 361 (2010) 180–186.
- [35] H. Wang, L. Ma, K. Cao, J. Geng, J. Liu, Q. Song, X. Yang, S. Li, Selective solid-phase extraction of uranium by salicylideneimine-functionalized hydrothermal carbon, *J. Hazard. Mater.*, 229–230 (2012) 321–330.
- [36] F.M. Oliveira, B.F. Somera, M.Z. Corazza, M.J.S. Yabe, M.G. Segatelli, E.S. Ribeiro, E.C. Lima, S.L.P. Dias, C.R.T. Tarley, Cellulose microfibril functionalized with N,N'-bis(2-aminoethyl)-1,2-ethanediamine as a solid sorbent for the fast preconcentration of Cd(II) in flow system analysis, *Talanta*, 85 (2011) 2417–2424.
- [37] S.S. Tahir, N. Rauf, Thermodynamic studies of Ni(II) sorption onto bentonite from aqueous solution, *J. Chem. Thermodyn.*, 35 (2003) 2003–2009.
- [38] V. Boonamnuayvitaya, C. Chaiya, W. Tanthapichakoon, S. Jarudilkul, Removal of heavy metals by adsorbent prepared from pyrolyzed coffee residues and clay, *Sep. Purif. Technol.*, 35 (2004) 11–22.
- [39] K. Li, Z. Liu, T. Wen, L. Chen, Y. Dong, Sorption of radiocobalt(II) onto Ca-montmorillonite: effect of contact time solid content pH ionic strength and temperature, *J. Radioanal. Nucl. Chem.*, 292 (2012) 269–276.
- [40] I. Langmuir, The adsorption of gases on plane surfaces of glass mica and platinum, *J. Am. Chem. Soc.*, 40 (1918) 1361–1403.
- [41] E.R. Sylwester, E.A. Hudson, P.G. Allen, The structure of uranium (VI) sorption complexes on silica, alumina, and montmorillonite, *Geochim. Cosmochim. Acta*, 64 (2000) 2431–2438.
- [42] V.K. Jain, A. Handa, S.S. Sait, P. Shrivastav, Y.K. Agrawal, Preconcentration, separation and trace determination of lanthanum(III), cerium(III), thorium(IV) and uranium(VI) on polymer supported *o*-vanillinsemicarbazone, *Anal. Chim. Acta*, 429 (2001) 237–246.
- [43] K. Dev, R. Pathak, G.N. Rao, Sorption behaviour of lanthanum(III), neodymium(III), terbium(III), thorium(IV) and uranium(VI) on Amberlite XAD-4 resin functionalized with bicine ligands, *Talanta*, 48 (1999) 579–584.
- [44] Y. Jung, S. Kim, S.J. Park, J.M. Kim, Application of polymer modified nanoporous silica to adsorbents of uranyl ions, *Colloids Surf., A*, 313–314 (2008) 162–166.
- [45] Y. Liu, Y. Liu, X. Cao, R. Hua, Y. Wang, Q. Li, Temperature swing adsorption of uranium(VI) ions on poly(N-isopropylacrylamide)/chitosan semi-IPN, *Int. J. Nucl. Energy Sci. Eng.*, 1 (2011) 8–14.
- [46] A.M. Donia, A.A. Atia, A.M. Daher, O.A. Desouky, E.A. Elshehy, Selective separation of U(VI) from its solutions using amine modified silica gel produced from leached zircon, *Int. J. Miner. Process.*, 101 (2011) 81–88.
- [47] X. Wang, L. Xia, K. Tan, W. Zheng, Studies on adsorption of uranium (VI) from aqueous solution by wheat straw, *Am. Inst. Chem. Eng.*, 31 (2011) 566–576.
- [48] T.S. Anirudhan, J. Nima, P.L. Divya, Adsorption and separation behaviour of uranium(VI) by 4-vinylpyridine-grafted-vinyltriethoxysilane-cellulose ion imprinted polymer, *J. Environ. Chem. Eng.*, 3 (2015) 1267–1276.
- [49] H.M.F. Freundlich, Over the adsorption in solution, *Z. Phys. Chem.*, 57 (1906) 385–471.
- [50] M.J. Temkin, V. Pyzhev, Recent modification to Langmuir isotherms, *Acta Physicochim.*, USSR, 12 (1940) 217–222.
- [51] Y. Niu, R. Qu, C. Sun, C. Wang, H. Chen, C. Ji, Y. Zhang, X. Shao, F. Bu, Adsorption of Pb(II) from aqueous solution by silica-gel supported hyperbranched polyamidoamine dendrimers, *J. Hazard. Mater.*, 244–245 (2013) 276–286.
- [52] X. Song, Y. Niu, P. Zhang, C. Zhang, Z. Zhang, Y. Zhu, R. Qu, Removal of Co(II) from fuel ethanol by silica-gel supported PAMAM dendrimers: combined experimental and theoretical study, *Fuel*, 199 (2017) 91–101.
- [53] A. Shahbazi, H. Younesi, A. Badiei, Batch and fixed-bed column adsorption of Cu(II) and Cd(II) from aqueous solution onto functionalized SBA-15 mesoporous silica, *Can. J. Chem. Eng.*, 91 (2013) 739–750.
- [54] S. Singha, U. Sarkar, S. Mondal, Transient behavior of a packed column of *Eichhornia crassipes* stem for the removal of hexavalent chromium, *Desalination*, 297 (2012) 48–58.
- [55] R. Han, D. Ding, Y. Xu, W. Zou, Y. Wang, Y. Li, L. Zou, Use of rice husk for the adsorption of Congo red from aqueous solution in column mode, *Bioresour. Technol.*, 99 (2008) 2938–2946.
- [56] H. Thomas, Heterogeneous ion exchange in a flowing system, *J. Am. Chem. Soc.*, 66 (1994) 1664–1666.
- [57] Y. Yoon, J. Nelson, Application of gas adsorption kinetics I. A theoretical model for respirator cartridge service time, *Am. Ind. Hyg. Assoc. J.*, 45 (1984) 509–516.
- [58] A. Shahbazi, H. Younesi, A. Badiei, Functionalized SBA-15 mesoporous silica by melamine-based dendrimer amines for adsorptive characteristics of Pb(II), Cu(II) and Cd(II) heavy metal ions in batch and fixed bed column, *Chem. Eng. J.*, 168 (2011) 505–518.
- [59] J.T. Nwabanne, P.K. Igbokwe, Adsorption performance of packed bed column for the removal of lead(II) using oil palm fibre, *Int. J. Appl. Sci. Technol.*, 2 (2012) 106–115.